Preparation and Characterization of the Nanocomposites from Chemically Modified Nanocellulose and Poly(lactic acid)

Liqing Wei[1], Shupin Luo[2], Armando G. McDonald[2], Umesh P. Agarwal[1], Kolby C. Hirth[1], Laurent M. Matuana[3], Ronald C. Sabo[1]* and Nicole M. Stark[1]*

[1]*USDA Forest Service, Forest Products Laboratory, One Gifford Pinchot Drive, Madison, WI 53726, United States*
[2]*Renewable Materials Program, Department of Forest, Rangeland and Fire Sciences, University of Idaho, Moscow, ID 83844-1132, United States*
[3]*School of Packaging, Michigan State University, East Lansing, MI 48824, United States*

Received March 01, 2017; Accepted April 23, 2017

ABSTRACT: Cellulose nanocrystals (CNCs) are renewable and sustainable filler for polymeric nanocomposites. However, their high hydrophilicity limits their use with hydrophobic polymer for composite materials. In this study, freeze-dried CNCs were modified by transesterification with canola oil fatty acid methyl ester to reduce the hydrophilicity. The transesterified CNCs (CNCFE) were compounded with PLA into nanocomposites. CNCFE with long-chain hydrocarbons plays a role as plasticizer. Increasing CNCFE loadings resulted in clear plasticizing effects. Lower T_g and T_m were achieved for CNCFE-based nanocomposites. Plasticizing nanocomposite melt with CNCFE can mitigate the degradation of CNCs during thermal processing. The elongation at break of nanocomposites containing 5% CNCFE was increased. Dynamic rheological study showed the highest elastic and viscous moduli (G′ and G″) and complex viscosity (G*) of nanocomposites with addition of 2% CNCFE. By tailoring the loadings of the transesterified CNCs, tunable structure and properties of nanocomposites can be obtained.

KEYWORDS: Nanocellulose, modification, nanocomposites, characterization

1 INTRODUCTION

Driven by awareness to develop eco-friendly products, there is a desire to replace the conventional polymer matrix materials with biobased polymers. Biobased polymer offers various advantages such as eco-efficiency, renewability, and most importantly, promising biodegradability so that the polymer can fully decompose at the end of its life. The most commonly known biobased polymers in today's marketplace include polyhydroxyalkanoates, polylactic acid (PLA), starch- and soy protein-based resins, bio-polyethylene, and bio-polypropylene [1]. Of these, PLA is the most widely used because of its high transparency and increased production. However, PLA has low impact strength, high brittleness (less flexibility), low crystallization rate and degree, and low thermal stability, limiting its industrial applications [2]. In order to improve the flexibility of PLA, glycerol-based plasticizers have been used [3]. The plasticizing effect was reflected by lower glass transition temperature (T_g) and facilitated cold crystallization ability. Recently, long-chain octyl epoxy stearate (OES) has also attracted interest as an alternative plasticizer to toughen PLA [4]. However, leaching of additives and processing aids is another driving force to develop sustainable and green modification strategies.

One potential solution to improve the thermomechanical properties of PLA is the inclusion of cellulose nanocrystals (CNCs), also known as cellulose whiskers, nanowhiskers, or nanorods. CNCs are produced through transverse cleavage of cellulose by acid hydrolysis to remove the amorphous region [5]. This gives CNCs a high modulus of around 170 GPa, showing the great potential of CNCs for reinforcing polymer matrix [6]. Similar to traditional cellulose fibers, the abundant hydroxyl groups on CNC surfaces make it a highly hydrophilic material. Hence, water-soluble matrix polymers, such as poly(vinyl alcohol) and

**Corresponding authors*: nstark@fs.fed.us; rsabo@fs.fed.us

DOI: 10.7569/JRM.2017.634144

poly(ethylene oxide) [7, 8], have been commonly used to prepare nanocomposites in a water medium.

The biggest obstacle for the practical application of nanocomposites from CNCs and hydrophobic polymer is the poor stress transfer between the two phases [9]. Poor compatibility leads to nanocomposites being vulnerable to environmental attacks such as water absorption, biodeterioration, and mechanical failure at interfaces. Another limitation for CNCs as reinforcement in polymer matrix is that CNCs tend to aggregate during the drying process due to high surface area and surface energy [10]. Nanocomposites from CNCs and hydrophobic polymers have been mostly prepared by organic solvent cast to attain a reasonable dispersion of CNCs in the polymer matrix. Nevertheless, melt processing is the more applicable, scalable and commercial technique for manufacturing polymer composites, but there are some challenges for surface interaction between polymers and CNCs [11, 12].

In order to broaden the application of nanocellulose and improve the hydrophobicity and compatibility at the polymer/nanocellulose interface, various chemical modifications have been applied, such as silylation [13], acetylation [14] and additives such as surfactant and plasticizer [15, 16]. However, those mentioned strategies mostly employed organic solvents or toxic reagents. Moreover, separately added plasticizers used to improve flexibility of the PLA-based composite can leach from the polymer matrix during service and lead to an environmental issue when discarded at the end of life [17].

The transesterification of vegetable oil with short-chain alcohols, in the presence of base catalyst, can be used to obtain the long-chain fatty acid methyl ester (FAME). The hydrophobic long-chain hydrocarbon structure could be chemically bonded to CNCs by the second transesterification reaction between the hydroxyl (OH) groups and FAME. From the perspective of polymer melt processing, the most favorable property of vegetable oil fatty acid is that long-chain hydrocarbons could play a role similar to a plasticizer by enhancing the flexibility of nanocomposites. Compared with separately adding a plasticizer, the leaching issue of the plasticizer could potentially be overcome by this novel proposed transesterification method using FAME. Reduced hydrophilicity, improved CNC dispersion and enhanced compatibility at the interfaces of filler/polymer may be achieved. To our knowledge, this type of transesterification has not been studied for the modification of cellulose, including nanocellulose. In our recent study [18], canola oil fatty acid methyl ester was successfully used to modify CNC surfaces without using any toxic solvent, and reaction residues can be reused for the next batch of modification. The crystalline structure was retained during the modification, and the modified CNCs showed significantly hydrophobic surfaces as compared to unmodified CNCs.

In this study, FAME of canola oil was prepared and then used to produce transesterified CNCs under the optimized reaction conditions previously explored by us. The modified CNC was compounded as reinforcement/biofiller to the PLA matrix for nanocomposites for the first time. Surface morphology, crystalline structure, thermal, mechanical, and rheological properties of nanocomposites with different nanocellulose loadings were evaluated by SEM, XRD, DSC, tensile, and dynamic rheological tests. This study has focused on the plasticizing effect of transesterified CNCs on the properties and processability of PLA-based nanocomposites, which would broaden the CNCs applications as reinforcement and/or modifier for nanocomposites with favorable properties.

2 MATERIALS AND METHODS

A more detailed experimental section is provided in the Supplementary Material (SM).

2.1 Materials

Cellulose nanocrystals (CNCs) were produced by the USDA Forest Service, Forest Products Laboratory (Madison, Wisconsin) using 64% sulfuric acid hydrolysis method from prehydrolyzed kraft rayon-grade dissolving wood (*southern pine*) pulp (acid:cellulose = 8:1 [v:w]) as described elsewhere [19]. CNCs have the average length and width of 78 ± 30 nm and 11 ± 2 nm, respectively [18]. The liquid CNC suspension (10.7 wt%) was freeze-dried for one week to obtain dry CNC materials (0.94 wt% sulfur in sodium form). PLA pellets (Ingeo™, 4044D, density of 1.24 g/cm^3, and melt flow index of 3.3 g/10 min) were purchased from NatureWorks LLC (Minnetonka, MN, United States). PLA pellets were dried under vacuum prior to use. The number- and weight-average molecular weights (M_w = 113,000 g/mol; M_n = 92,500 g/mol) of PLA were determined by size exclusion chromatography (SEC) with details provided in the Supplementary Material. Other ACS grade chemicals were directly used as received without purification.

2.2 Transesterification of CNCs

Canola oil fatty acid methyl ester (CME) was first synthesized by the reaction of canola oil with excess methanol (MeOH) (molar ratio of methanol to canola oil = 6:1), following the modified method reported elsewhere [20]. Long-chain fatty acid methyl ester

 DOI: 10.7569/JRM.2017.634144

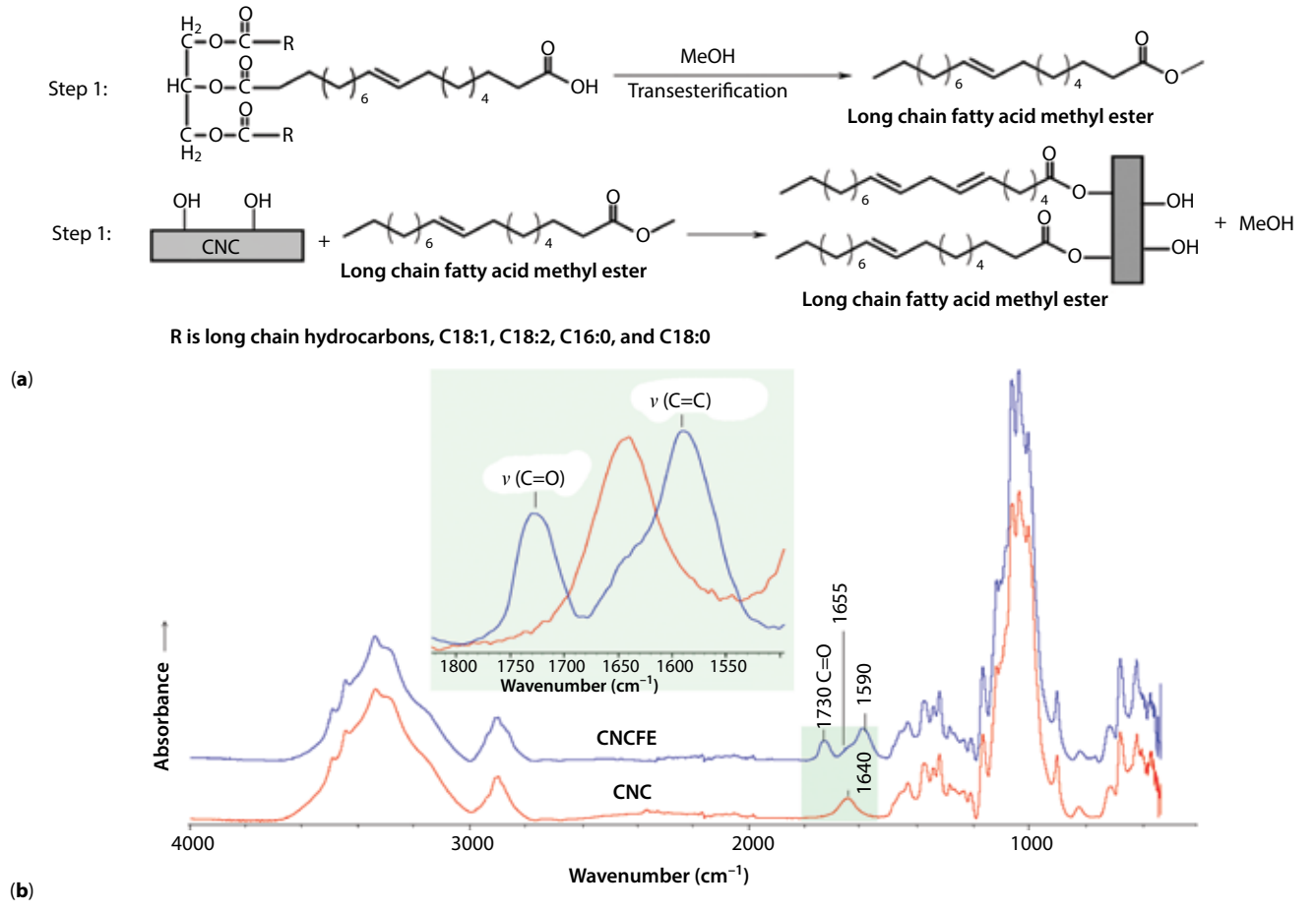

Figure 1 Reaction mechanism for the productions of CME and CNCFE (**a**) and FTIR spectra of unmodified CNCs and CNCFE (**b**).

of CNCs (CNCFE) was synthesized by the transesterification method that we have reported previously [18, 21]. The reaction mechanism is shown in Figure 1a. The CNCFE was selected from the batch with the following reaction conditions: reaction time = 20 h, reaction temperature = 120 °C, and the degree of OH substitution was equal to 0.5 mmol/g dry CNCs. After the reaction, CNCFE was recovered by centrifugation (5000 rpm) for 10 min, followed by Soxhlet extraction with hexane for 20 h to remove any non-reacted CME.

2.3 Nanocomposites Preparation

Injection molded PLA/CNC and PLA/CNCFE nanocomposites were prepared using a microprocessing system (DSM Xplore, DSM Research, Geleen, The Netherlands). The system consists of a 15 mL conical twin-screw compounder and a 12 mL injection molder. The compounding temperature was 185 °C and purged with N_2 to limit the degradation of PLA and nanocellulose. An ASTM D638 type V tensile property mold was used with the injector temperature set at 185 °C. Neat PLA samples were manufactured in the same method as nanocomposites material without adding CNC/CNCFE. Nanocomposite samples are coded based on their formulation: PLACNC-2, PLACNC-5, PLACNCFE-2, and PLACNCFE-5, which stand for nanocomposites containing 2% CNC, 5% CNC, 2% CNCFE, and 5% CNCFE, respectively.

2.4 Characterization

2.4.1 *Chemistry of Modified CNCs*

The surface chemistry changes of CNCFE samples were characterized by FTIR spectroscopy using a Thermo Nicolet iZ10 FTIR-ATR spectrometer (Thermo Scientific, Verona, WI). Spectra were taken for 128 scans in the range of 4000–600 cm^{-1} with the resolution of 4 cm^{-1}.

2.4.2 Morphology of Composites

Nanocomposites were microtomed to remove the surface layer of PLA plastic and coated with a thin layer of gold, and then investigated using a LEO Gemini field emission SEM operating at 3 kV under high vacuum.

2.4.3 Crystalline Structure by WAXD

The crystalline structures of unmodified CNCs, CNCFE, and nanocomposites were characterized by wide-angle X-ray diffraction (WAXD) spectroscopy (D8 Discover diffractometer, Bruker AXS Inc., WI, USA). The instrument was set up with a rotating Cu Kα2 X-ray IMS tube operating at 50 kV and 1000 μA. Scanning was performed over a 2θ range from 5 to 60° with steps of 0.005°. The collected diffractograms were processed and peaks of interest were fitted (Gaussian function) using IGOR Pro v6 software. The intensity of each peak identified by peak fitting was mathematically computed. The crystallinity index of nanocrystals (CNC and CNCFE, $CrI\%_{CNC/CNCFE}$) and PLA ($CrI\%_{PLA}$), crystal size dimensions (D_{hkl}) and the spacing between the (110)/(200) and (015) planes (d), were calculated according to Eqs. S1–S4 (Supplementary Material).

2.4.4 Differential Scanning Calorimetry (DSC)

The DSC analysis was performed using a TA Instruments model Q2000 DSC with refrigerated cooling. Approximately 5 mg samples were weighed in aluminium pans and subjected to two heating and one cooling scan from 0 to 200 °C at 10 °C/min. The degree of crystallinity (χ_c%) of PLA was calculated based on Eq. S4 (Supplementary Material) [22, 23].

2.4.5 Tensile Test

The tensile testing of injection molded nanocomposite samples was performed at 23 °C and 50% relative humidity using an Instron 5865 system (Instron Engineering Corp., MA, USA) with a 500 N load cell. The tests were performed with a crosshead speed of 1 mm/min. Ten specimens were tested for each sample. The grip section of the injection molded tensile specimens was cut off, and the density (ρ, g/cm^3) was calculated based on the initially conditioned dry weight and dimensions of the rectangular bars. Significance in the density and mechanical properties differences were statistically analyzed employing a Tukey's test. More detailed testing procedures are provided in the Supplementary Material.

2.4.6 Rheological Property

The dynamic rheological measurements (G′, G″, and η*) were performed on a Bohlin CVO 100 rheometer, a parallel plate (25 mm Ø), in an oscillating shear mode with an ETC module on molded disc (2 mm × 25 mm Ø) samples. Experiments were performed in the linear viscoelastic region. Measurements were carried out at 180 °C in the frequency range of 0.1 to 100 rad/s at an applied isostrain of 0.5%. Data were analyzed using the Bohlin rheology v6.51 software.

3 RESULTS AND DISCUSSION

3.1 Surface Chemistry of CNCFE and Morphology of Nanocomposites

As indicated by the FTIR spectroscopic analysis (Figure 1b), carbonyl groups were assigned to the aliphatic esters for CNCFE at 1730 cm^{-1} [24]. No peak was observed at 2853 cm^{-1} (O-CH_3 stretch), suggesting that the CME was removed completely by hexane extraction. This confirms that the long-chain hydrocarbons of CME have been successfully grafted onto CNC surfaces. The SEM micrographs for neat PLA and nanocomposites are shown in Figure 2. The PLA surface was flat and smooth (Figure 2a). In the PLA/CNCs nanocomposites (Figure 2b) the PLA polymer melt cannot infiltrate through the compact and dense structure of CNC agglomerates. Although the shear force during extrusion is not sufficient to disperse the agglomerates

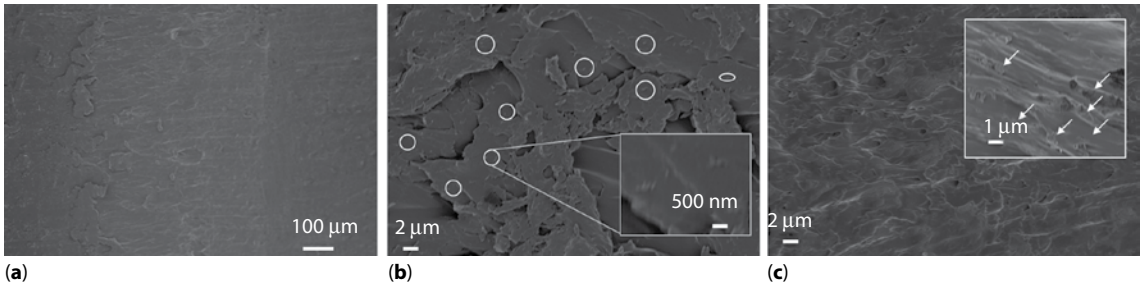

Figure 2 Scanning electron micrographs of microtomed surfaces of neat PLA (**a**), PLACNC-5 (**b**) and PLACNCFE-5 (**c**).

 DOI: 10.7569/JRM.2017.634144

into the PLA matrix, some small fragments (nanoscale) were detached, as shown in circles in Figure 2b (see the inset micrograph). A similar phenomenon was observed in polypropylene and freeze-dried CNCs nanocomposites system [25]. The flatter surface of the nanocomposite PLACNC-5 (Figure 2b) as compared to the PLACNCFE-5 nanocomposites (Figure 2c) is indicative of a more brittle fracture event, suggesting that incorporation of CNCs makes the PLA more brittle. Discrete/incontinuous zones and cavities are observed in PLACNC-5 when CNCs were presumably pulled out during microtoming (Figure 2b). This might be attributed to poor interfacial bonding and compatibility between the hydrophilic unmodified CNCs and hydrophobic PLA matrix. In addition, the dispersion of the unmodified CNCs was poor (Figure 2b) in polymer matrix, which is one of the drawbacks to using freeze-dried CNCs as biofiller/reinforcing agents for polymeric composites. This likely contributed to the large agglomerates/aggregates of freeze-dried CNCs and the poor bonding at the interface due to the high hydrophilicity of unmodified CNCs and the hydrophobicity of PLA matrix. In contrast, the interfacial adhesion and compatibility between CNCFE and PLA matrix may have been improved, as indicated by the increased microductility and plastic deformation and no apparent phase separation as a result of the better dispersion of CNCFE in PLA (Figure 2c).

3.2 Crystalline Structure

The crystalline structure of neat PLA and the effect of transesterification on the crystalline structures of nanocomposites were investigated by WAXD analysis. The diffractograms and patterns are shown in Figure 3. Neat PLA had crystalline peaks at 15.4°, 17.1°, 19.5°, 22.9°, and 29.8°, respectively, corresponding to planes of (010), (110)/(200), (203), (015), and (1010) of PLA α-crystals [26]. Though crystalline peaks of CNC/CNCFE are not apparent in the nanocomposites due to low levels of addition, they can contribute to peak broadening of nanocomposites as compared to pure PLA. It is worth noting that the crystalline structure was not altered due to modification, as indicated in our previous study [18]. All of the PLA crystalline peaks appeared in the nanocomposites except for PLACNCFE-5, for which only the peak at 16.9° was clearly seen. A broadening pattern was observed for PLACNCFE-5, which indicates the PLA crystal structure in PLACNCFE-5 sample was distorted due to the positive plasticizing effect on the nanocrystal (CNCFE) dispersion within the polymer matrix [27].

The Gaussian function was used for peak fitting of the XRD diffractograms. The results obtained from fitted peaks of peak angle (2θ), FWHM, average crystal size (D_{hkl}) in the direction perpendicular to the reflection plane and crystallinity index, $CrI\%_{PLA}$, are listed in Table 1. Adding 2% unmodified CNCs resulted in higher $CrI\%_{PLA}$ (25.5%) compared to PLA (19.8%). Smaller crystal sizes ($D_{110/200}$ and D_{015}) were obtained for PLACNC-2 ($D_{110/200}$ = 82; D_{015} = 138) and PLACNC-5 ($D_{110/200}$ = 48; D_{015} = 37) than neat PLA ($D_{110/200}$ = 83; D_{015} = 139). Kamal and Khoshkava found that spray-dried CNCs played a role as a nucleation agent, resulting in an increased crystallization rate of PLA in the nanocomposites [28], which is consistent with the results in this study. Since CNCs could stimulate the crystallization rate during the injection molding process, there could be insufficient time for the PLA melt to form larger crystals. Additionally, the existence of

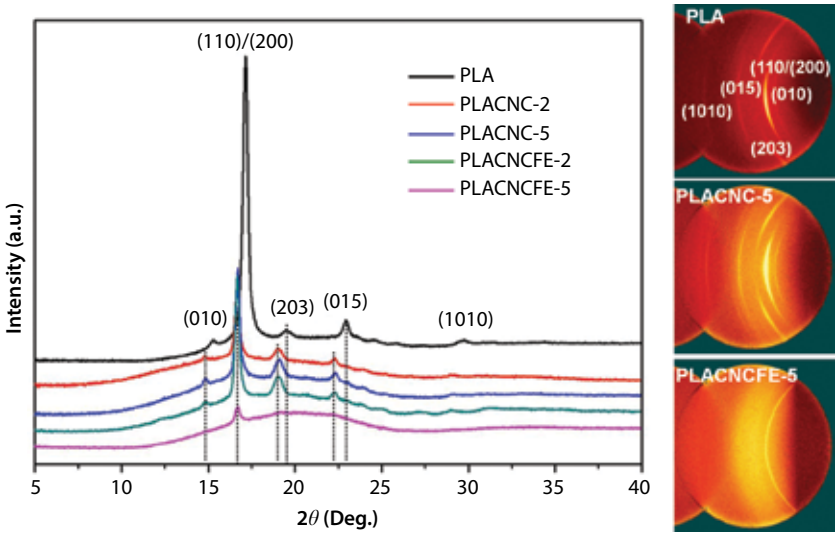

Figure 3 XRD diffractograms and patterns of neat PLA and nanocomposites.

Table 1 Crystalline parameters and thermal properties determined from XRD and DSC.

	XRD					DSC					
	2θ	FWHM (°)	d (Å)[a]	$D_{110//200}$,D_{015} (Å)[a]	$CrI\%_{PLA}$	T_g (°C)	T_{cc} (°C)	T_m (°C)	ΔH_{cc} (J/g)	ΔH_m (J/g)	χ_c (%)
PLA	17.1	0.967	10.3	83	19.8	60.4	117.6	148.9	17.1	21.2	4.4
	22.9	0.583	7.9	139							
PLACNC-2	16.7	1.366	10.6	82	25.5	60.3	118.0	147.9	11.7	21.0	10.1
	22.2	0.666	8.0	138							
PLACNC-5	16.7	1.665	10.6	48	22.7	60.3	120.0	148.9	10.2	17.5	8.2
	22.2	2.165	8.0	37							
PLACNCFE-2	16.7	1.332	10.6	60	14.0	42.1	96.5	138.6, 148.1	20.6	23.7	3.3
	22.5	1.330	7.9	61							
PLACNCFE-5	16.7	2.665	10.6	30	5.0	42.0	102.0	138.0, 147.3	19.2	22.1	3.2
	22.0	2.997	8.1	27							
PLA-CME						42.3	96.3	137.6, 147.4	19.2	22.6	3.8

[a] Crystal sizes (D_{hkl}) and *d* spacing were determined in the direction perpendicular to the planes of (110)/(200) and (015) of PLA.

micron-scale CNCs could also hinder the linear PLA polymer chains to be folded. When the CNC content was increased to 5%, the crystal sizes of nanocomposites (PLACNC-5) were reduced further and the crystallinity was slightly lower ($CrI\%_{PLA}$ = 22.7%) than that of PLACNC-2 sample (Table 1). Although agglomerates are present in the freeze-dried CNCs, relatively more of the smaller CNCs were detached by extrusion shear force (Figure 2c). The $CrI\%_{PLA}$ of PLACNC-5 was lower than PLACNC-2, possibly due to the percolation threshold of the unmodified CNCs volume in the polymer matrix. In other words, if the CNCs loading exceeds a certain level the crystallization of PLA would be hindered. Dramatic reduction in crystallinity and crystal sizes for CNCFE-based nanocomposites, especially for PLACNCFE-5 sample ($CrI\%_{PLA}$ = 5.0 %; $D_{110/200}$ = 30; D_{015} = 27), is suggested by peak broadening of all crystalline planes (Figure 3). Such results can be explained by the presence of long-chain hydrocarbons covalently attached to the CNCFE surfaces, which would suppress the nucleation of the polymer. The effect of plasticizing was positively correlated with CNCFE content.

3.3 Thermal Properties

The thermal events of glass transition temperature (T_g), cold crystallization (T_{cc}) and melting transition (T_m) of neat PLA and nanocomposites were studied by DSC. The second heating thermograms are shown in Figure 4. Thermal transitions and crystallization/melting enthalpy as well as the degree of crystallinity (χ_c%) of the materials are summarized in Table 1. Neat PLA showed a T_g = 60.4 °C and a single endothermic peak at T_m = 148.9 °C. The addition of CNC to PLA (PLACNC-2 and PLACNC-5) had virtually no effect on the T_g and T_m, which is likely due to the poor compatibility between unmodified CNCs and polymer matrix [29]. However, the 2% CNCFE-based nanocomposites (PLACNCFE-2) reduced T_g by 18.3 °C. Further addition of CNCFE did not result in additional changes to T_g or T_m. Since T_g is directly associated with the macromolecular mobility of polymer chains, the lower T_g transits the CNCFE-based nanocomposites from a glassy to a rubbery state. In other words, at room temperature, as prepared PLA and CNCFE nanocomposites are more ductile (less rigid). This behavior is attributed to the plasticizing effect of the long-chain hydrocarbon structure of the fatty acid ester side of the transesterified CNCs. As postulated in Figure 5, these hydrocarbon molecular chains are covalently bonded to the CNC surfaces, and then embedded between chains of PLA during the polymer melt process. The widened space of PLA polymer chains increases "free volume," and thus significantly lowers the T_g for PLA. The space depends on the length of the hydrocarbons grafted and the arrangement of those long chains, which is mainly determined by the composition of canola oil fatty acids. Our previous study found that there are respectively 66.6% of C18:1, 23.8% of C18:2, 6.8% of C18:3, 1.8% of C16:0, and 1.0% of C18:0 [18]. Therefore, if these components randomly reacted with

 DOI: 10.7569/JRM.2017.634144

CNCs in their methyl ester form, about 98.2% of C18 and 1.8% of C16 have been grafted onto CNCs.

The degree of crystallinity of the injection molded materials was determined by subtracting the enthalpies for cold crystallization from the melting enthalpy (Figure 4). As a consequence of the small sizes of CNCs, the enhanced nucleation effect was achieved and therefore slightly higher χ_c% was obtained for PLACNC-2 (10.1%) and PLACNC-5 (8.2%) with respect to PLA (4.4%). There was no additional increase of χ_c% when the CNCs content was increased from 2 to 5%, indicating that when the volume ratio of the freeze-dried CNC large aggregates exceeds a percolation threshold the crystallization of PLA from melt would be hindered. This is consistent with the results of $CrI\%_{PLA}$ from WAXD results. Increased mobility for plasticized polymer chain in PLACNCFE nanocomposites resulted in a larger portion of the amorphous phase that was more readily able to cold crystallize during the heating scan. This is reflected by larger cold crystallization enthalpy (ΔH_{cc}) values (Figure 4 and Table 1) for PLACNCFE composites compare to PLA and PLACNC. As a consequence, larger melting enthalpy (ΔH_m) values were observed for PLACNCFE nanocomposites than for PLA and PLACNC nanocomposites, while lower χ_c% values of PLACNCFE nanocomposites were obtained. This agrees with the trend of WAXD results. However, higher χ_c% values of plasticized PLA-based nanocomposites were reported elsewhere [16,30], which was ascribed not just to higher mobility of polymer chains but also better dispersion of nanofillers. It is difficult for plasticized polymer chains to be aligned into ordered structures possibly led by molecular chain slippage. Perhaps competing effects of crystal nucleation effect due to nanoscale fillers and inhibited ordering of plasticized polymer chains are at play. Hence, the concentration of CNCFE can potentially be adjusted to tune the plasticizing effect in nanocomposites to meet various requirements for T_g and χ_c% for different applications.

As a result of the increased "free volume," heat fusion into the nanocomposites system would be more effective, giving lower T_m values of PLACNCFE-2 and PLACNCFE-5 as compared to neat PLA and unmodified CNCs-based nanocomposites. For PLACNCFE-2 and PLACNCFE-5 nanocomposites, double endothermic peaks (T_{m1} = 138.6 °C and T_{m2} = 149.1 °C, labeled from low to high temperature in Figure 4d and 4e) corresponding to melting temperatures were observed. In order to better explain the origins of the two melting peaks, PLA plasticized with 1% CME (PLA-CME) was measured with DSC as a comparison. Double melting peaks were seen in the PLA-CME sample as well with T_{m1} (137.6 °C) and T_{m2} (147.4 °C) values close to those observed in PLACNCFE-2 and PLACNCFE-5. This further confirmed the plasticizing effect of the CNCFE to the PLA matrix. Martin and Avérous [3] found a similar double melting behavior when PLA was plasticized by glycerol and polyethylene glycol. It is speculated that there could be two types of crystalline structures present in the CNCFE-based nanocomposites [3]. The lower temperature endotherm might be attributed to the secondary crystallization resulting from lamellar rearrangement. The peak at higher temperature was

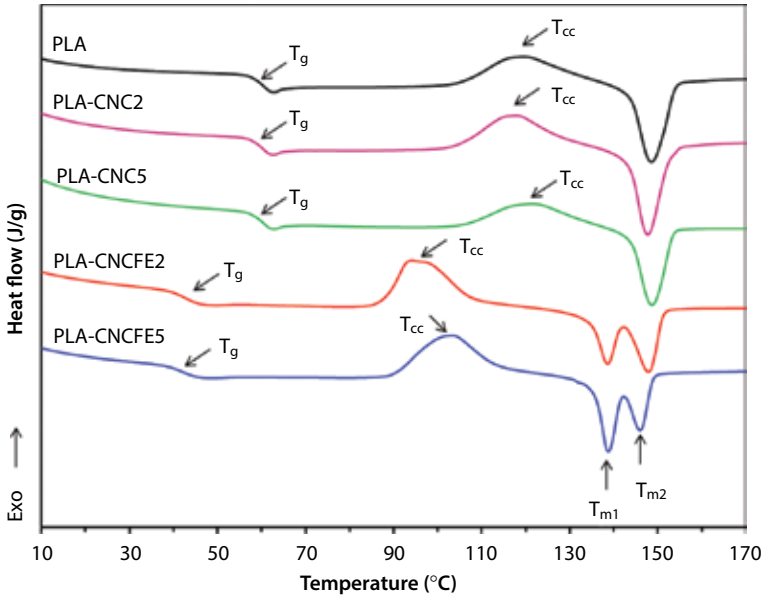

Figure 4 DSC thermograms of (**a**) PLA, (**b**) PLACNC-2, (**c**) PLACNC-5, (**d**) PLACNCFE-2, (**e**) PLACNCFE-5, and (**f**) plasticized PLA by CME (PLA-CME).

the melting of original PLA crystals. Since more plasticizing effect is expected with increased CNCFE loading, it is not surprising to see that the PLACNCFE-5 had larger amplitude (area) of the lower endothermic peak than that of the PLACNCFE-2.

The T_{cc} is an important parameter to describe the cold crystallization behavior of composites. This peak shifted from 117 °C for PLA to 118 °C and 120 °C for PLACNC-2 and PLACNC-5, respectively, indicating the delay of crystallization with incorporation of CNCs. However, addition of 2% and 5% CNCFE reduced the T_{cc} of nanocomposites by 23.5 °C and 15 °C, respectively. This suggests that the plasticizing effect promoted crystallization ability via enhancing polymer chain mobility. This is also a good indicator of the improved melting processability of PLACNCFE nanocomposites [23, 31].

3.4 Tensile Deformation Properties

Influences of transesterification on the tensile properties of the nanocomposites are shown in Figure S1 and Table 2. The density of the nanocomposites remains similar to PLA, which may be because only low fractions (2% and 5%) of CNCs have been used in the composites.

Adding 2% CNC or CNCFE did not affect the modulus of PLA significantly but adding 5% of either filler increased it from 3.8 GPa to 5.1 GPa (Table 2). This suggests there could be a percolation threshold (volume fraction) of CNCs in the PLA matrix to perform as a true reinforcement for those CNC aggregates. No significant difference was observed between PLACNCFE-5 and PLACNC-5. A similar trend of E changes was observed for surfactant modified PLA/CNC nanocomposites [15]. In order to clarify the reinforcing effect of CNCs in this study, theoretically predicted values of Young's modulus of nanocomposites (E_c) was calculated by using Halpin-Tsai equations (Supplementary Material, Eqs. 5–8). Results are given in Table 2. Before freeze-drying process, the CNC aspect ratio (L/d) was about 8 [18]. If assuming the CNC morphology was not changed during the drying process, the predicted E_C values of PLACNC-2 and PLACNC-5 were 4.5 and 5.5 GPa, respectively, larger than the corresponding experimental E values. However, the freeze-dried CNCs lost the rod-like morphology and became sheet- or

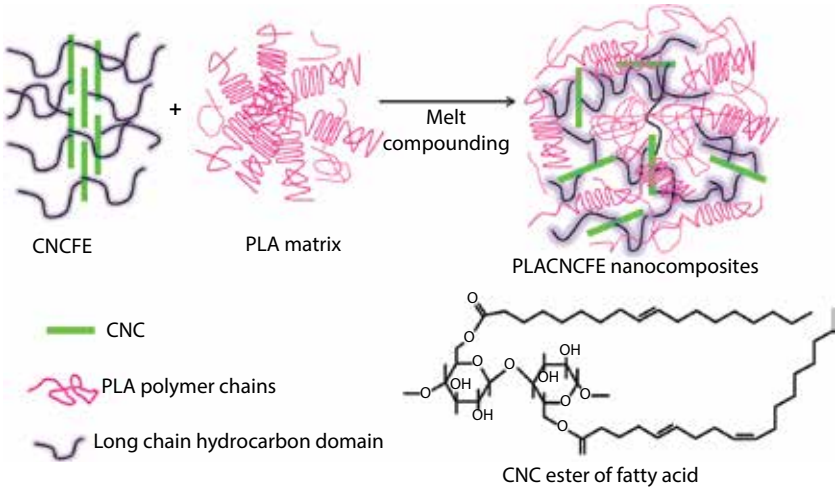

Figure 5 Illustration of plasticizing effect of long chain hydrocarbon of CNCFE in nanocomposites.

Table 2 Density (ρ) and tensile results of PLA and nanocomposites. Standard error values are given in parentheses. Samples with same letter are not significantly different at 95% confidence interval of probability using Tukey's paired t-tests.

Sample	ρ (g/cm³)	E (GPa)	E_C (GPa)	Ec^* (GPa)	σ (MPa)	ε (%)
PLA	1.25 (0.1)[a]	3.8 (0.7)[a]	--	--	64.6 (2.2)[a]	7.6 (1.2)[a]
PLACNC-2	1.19 (0.1)[a]	4.3 (0.4)[a]	4.5	3.9	58.9 (1.1)[b]	2.5 (0.3)[b]
PLACNC-5	1.21 (0.1)[a]	5.1 (0.3)[b]	5.5	4.1	59.8 (0.9)[b]	2.5 (0.3)[b]
PLACNCFE-2	1.21 (0.1)[a]	4.1 (0.2)[a]	--	--	41.9 (2.8)[c]	6.4 (1.0)[ab]
PLACNCFE-5	1.16 (0.1)[a]	5.1 (0.8)[b]	--	--	22.1 (0.5)[d]	20.1 (2.5)[c]

Note: E_C and E_C^* were obtained with L/d taken as 8 and 1, respectively.

flake-like large particles [18]. As observed in the SEM micrographs of the fracture surfaces of nanocomposites (Figure 6a and 6b), the aspect ratio (L/d) of freeze-dried CNCs is close to unity (1). Accordingly, the calculated modulus (E_c*) was 3.9 and 4.1, respectively, for PLACNC-2 and PLACNC-5. Herein, the experimental values are even higher than the theoretical results in this study. Hence, the ability of the freeze-dried CNCs as reinforcing material seemed to be fully exploited. The most probable reason why lower modulus values of PLACNC-2 lose the nature of ideal reinforcement in polymer matrix was that its aspect ratio was reduced significantly during the freeze-drying process. This is because the modulus of short fiber and polymer composites mainly depends on the morphology (rod-like or short fiber-like) of fiber and fiber content [23].

Lower stress (σ) values at the ultimate yield point were observed for CNCs-based nanocomposites than PLA, indicating the freeze-dried CNCs from high concentration of CNC suspension (10.7 wt%) in this study were not an ideal reinforcement for PLA. The σ of short fibers and polymer composites is more dependent on the filler-polymer interaction (compatibility). Hence, lower σ value of PLACNC-2 and PLACNC-5 than that of neat PLA was contributed to the hydrophilic surfaces of CNCs and hydrophobic PLA matrix. The addition of CNCFE showed lower σ value as compared to PLA and PLACNC nanocomposite. A similar decreasing trend of σ was also observed in limonene plasticized PLACNC nanocomposites systems [16]. This might contribute to the coupling effect of the better compatibility at the CNCFE/PLA interface and the plasticizing effects given by the long-chain hydrocarbons.

The ductility of the materials are reflected by elongation to break (ε, %) values (Table 2 and Figure S1a). With the addition of CNCs, lower ε values were observed. This is commonly seen in CNCs-based nanocomposites because of the poor stress transfer and severe stress concentration at the interface of unmodified CNCs and PLA matrix (Figure S1b), which leads to easier mechanical failure at filler/polymer interfaces. When 2% CNCFE was incorporated the ε was 6.4%. This suggests increased flexibility of nanocomposites by plasticizing as compared to unmodified CNCs-based nanocomposites. Furthermore, the ε was significantly increased to 20% when 5% CNCFE was incorporated, indicating that a more obvious plasticizing effect and better stress transfer at the filler/polymer interface is expected (Figure S1b). The fractured surfaces of nanocomposites showed that the relatively better CNCFE dispersion (Figure 6b) within the PLA matrix was observed as compared to that of the unmodified CNCs (Figure 6a). This could also be another main reason for the improved ductility and toughness of the resulting nanocomposites. Smaller CNCFE particle sizes were observed in the PLA matrix, which could indicate the more nucleating effect of the CNCFE particles than unmodified CNCs. This again suggests reduced strength of the PLACNCFE nanocomposites due to the plasticizing effect, which is commonly observed in plasticized CNC-reinforced polymers [16,30], and confirms our earlier assumption that there is a trade-off between nucleation and plasticizing effect. In addition, a lower degree of crystallinity and smaller crystal sizes, as determined above, could also be contributing factors to improved ductility. Hence, the mechanical properties of nanocomposites can potentially be tailored according to different applications by varying their formulation. This may suggest their prospective applicability as packaging films with demanding flexibility but lower mechanical strength. Nanoscaled CNC particles can be observed on the fractured surfaces after tensile measurements (Figure 6). In contrast, the CNCFE-based nanocomposite (Figure 6b) shows smaller particle sizes compared to unmodified CNC-based nanocomposites (Figure 6a). It seems the increased hydrophobicity of CNCFE could make it easier for PLA melt to attach onto CNCFE surfaces,

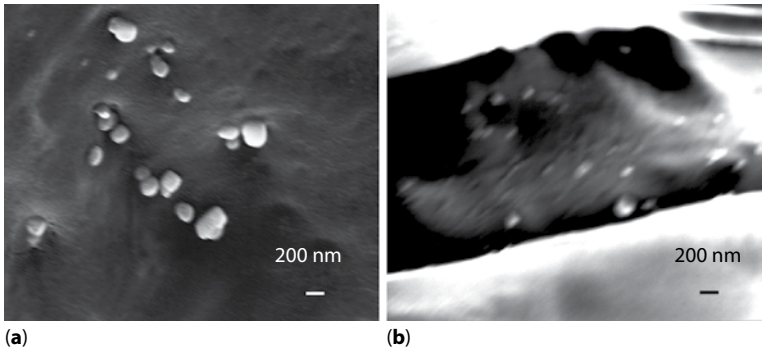

(**a**) (**b**)

Figure 6 Fracture surface of nanocomposites with 5% unmodified CNCs (a) and CNCFE (b).

and therefore improved dispersion of CNCFE within the PLA matrix was seen (Figure 6b).

3.5 Melt Strength and Rheological Properties

Polymer melt rheological properties of neat PLA and nanocomposites were determined by dynamic parallel plate rheometry. Figure 7 shows the dynamic moduli (G′ and G″) of materials under isothermal conditions. At lower frequency (ω, rad/s) the G′ was lower than G″. This indicates that these polymers show liquid-like relaxation behavior, although the incorporation of CNC and CNCFE crystals made the resulting nanocomposites melt more elastic, which was reflected by there being less difference (arrows in Figure 7) between G′ and G″ values at given ω. For PLACNC-2, PLACNC-5 and PLACNCFE-2, elasticity (G′) and loss modulus (G″) were seen to increase as compared to neat PLA. For instance, addition of 2% CNCFE to PLA (PLACNCFE-2) resulted in the G′ and G″ increasing from 1,580 to 5,060 Pa and 11,500 to 15,200 Pa, respectively, at 1 rad/s. This clearly shows that these nanocomposites had improved melt strength at the same isothermal conditions. This also indicates that regardless of the aggregated structures of freeze-dried CNCs, the effect of unmodified CNCs on the melt strength and/or melt processability of the resultant composites would be positive. The crossover point of G′ and G″ (G_c = G′ = G″) was shown to occur at a lower frequency (25 rad/s) for the PLACNCFE-2, while G_c of other samples all occurred at ω close to 41 rad/s. The G_c was increased from 62,100 Pa for PLA to 86,300 Pa by the addition of 2% CNCs and was further increased to 79,700 Pa for PLACNC-5. The G_c was increased to 78,800 Pa for PLACNCFE-2 whereas it was decreased to 40,400 Pa for PLACNCFE-5. It was seen that both G′ and G″ were reduced by incorporation of 5% CNCFE. This is caused by the more obvious plasticizing effect due to more of the long-chain hydrocarbons bonding to the nanocrystals, which would increase polymer chain slippage under applied deformation forces. Moreover, the reduction in moduli with angular frequency when CNCFE content was increased from 2 to 5% could suggest there could be a percolation threshold (volume fraction) of CNCFE in the PLA matrix regarding the processability of composite melt. It is worth noting that the slopes for both moduli in the terminal region were lower by adding unmodified and modified CNCs to PLA. For example, the slope of G′ versus frequency was decreased from 1.13 for PLA to 1.05 for PLACNC-5 and 0.09 for PLACNCFE-5. The weaker dependence of the modulus on the angular frequency, namely gentle slope, observed for nanocomposites is characteristic of solid-like behavior of polymer melt [25]. In addition, the elastic modulus of polymer melt is known to increase as temperature is reduced [32]. This suggests that lower processing temperature can be used for plasticized nanocomposites to obtain comparative or even higher polymer melt strength. It is therefore expected to broaden the melt

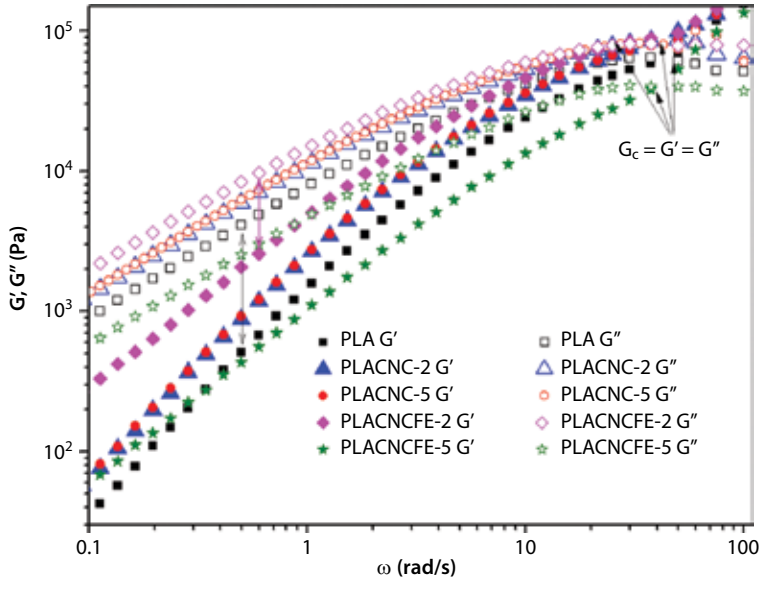

Figure 7 Dynamic rheology storage (G′) and loss (G″) moduli of neat PLA and nanocomposites. G_c is the crossover modulus when G′ = G″.

 DOI: 10.7569/JRM.2017.634144

processing window of these plasticized nanocomposites, such as by extrusion, injection molding, and film blowing.

The complex viscosity (η*) was increased upon addition of CNCs, however, no significant improvement of η* was observed when CNCs content was increased from 2% to 5%. Similar trends were observed in other nanocellulose filled polymer composites [25]. Nanocomposites with 2% CNCFE showed noticeable increased viscosity as compared to PLA, while 5% CNCFE decreased viscosity. The yield stress can directly indicate what stress level or driving force would transform the polymer melt from solid to liquid state. Hence, to obtain the yield stress from viscosity versus frequency seems to have the practical significance of showing the plasticity of polymer melt as compared to the moduli results. As shown in Figure 8a, the PLA melt displayed an apparent yield at lower frequency than nanocomposite samples. The relative yield stress (σ_0) was estimated by fitting the experimental data to a modified four-parameter Cross Model [25]:

$$\eta^* = \frac{\sigma_0}{\omega} + b \times \left(1 + c \times \omega^d\right)^{-1} \quad (1)$$

where b (Pa·s), c (s), and d (dimensionless) are model parameters. The fitted curves (R = 0.99 for all samples) are shown in Figure 8a as black lines and model

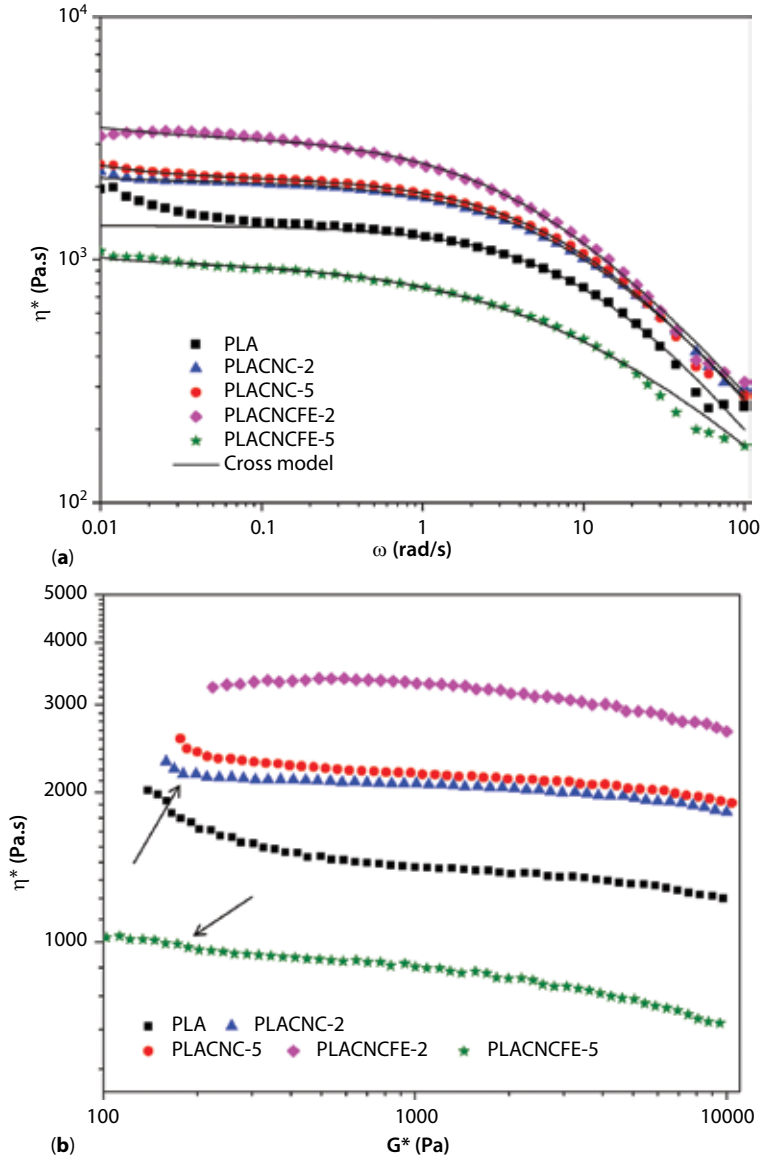

Figure 8 Dynamic rheology showing (**a**) complex viscosity (η*) vs. frequency (ω, rad/s) and (**b**) complex viscosity (η*) vs. complex modulus (G*) of neat PLA and nanocomposites. Note: arrows are showing the yielding regions.

parameters are given in Table S1. The σ_0 values are shown in the order of PLACNCFE-2 > PLACNC-5 > PLACNC-2 > PLACNCFE-5 > PLA.

These data further indicate that better nanocrystal dispersion in the PLA matrix can result in nanocomposites with improved melt plasticity [25]. The yield stress can be more obviously reflected by plotting complex viscosity (η*) as a function of complex modulus (G*) (Figure 8b). This confirmed that the PLA melt started to yield at lower frequency. The viscosity of polymer melt is associated with macromolecular chain structure changes due to the plasticizing effect by incorporation of 2% CNCFE. This means the plasticity threshold of the PLACNCFE-2 is rather high, while higher content of CNCFE in the PLACNCFE-5 nanocomposites resulted in PLA polymer with higher mobility and lower viscosity. These rheological results provide practical and fundamental information in the PLA/CNC or PLA/CNCFE nanocomposites subjected for thermal processing.

4 CONCLUSIONS

Cellulose nanocrystals were successfully transesterified using vegetable oil fatty acid methyl ester. Long-chain hydrocarbons were chemically bonded to CNCs and played a role as plasticizer. More obvious plasticizing effect was obtained with increased CNCFE loadings. The incorporation of 2% and 5% CNCFE can produce more ductile nanocomposites, as evidenced by reduced T_g, T_m and χ_c%. Addition of 5% CNCFE improved the elongation to break by 164% and 704% as compared to neat PLA and PLACNC-5, respectively. CNCFE resulted in nanocomposites that can be processed at lower temperatures because of the higher melt strength shown by dynamic rheological results, especially that of PLACNCFE-2. Overall, competing effects, such as reinforcement, plasticization and polymer crystallization, can potentially be controlled/manipulated to tailor composite properties. This indicated that such approaches allow for functionalizing nanocellulose reinforced water-insoluble polymer nanocomposites with tunable crystalline structure, thermal and mechanical properties and processability. Further investigations are expected to (i) determine if better particle/fiber morphology (in the nanoscale with $L/d >> 1$) would give reinforcement effect, (ii) reduce the competing effect of reinforcement and plasticizing effect of transesterified CNC, and (iii) determine the effect of modification on additional properties (e.g., barrier properties, durability, biodegradability, etc.) of the nanocomposites used for packaging materials and provide an outlet for the commercialization of cellulose nanomaterials.

ACKNOWLEDGMENT

The authors thank the funding from **Public-Private Partnership for Nanotechnology (P³Nano)** US Endowment for Forestry and Communities, Inc. (Grant No. CWFSCL15). We also acknowledge the following people from the USDA Forest Service, Forest Products Laboratory: Richard S. Reiner for preparing CNCs, Dr. Samuel L. Zelinka and Charles R. Boardman for the technical help with DSC, Dr. Craig Clemons, Neil Gribbins and Philip Walsh for help with Wiley mill, TGA and DSM system, and Sara Fishwild, Tim Nelson and Marshall Begel for assistance in tensile test and data analyses.

REFERENCES

1. L. Wei and A. McDonald, A review on grafting of biofibers for biocomposites. *Materials* **9**, 303 (2016).
2. S. Muniyasamy, O. Ofosu, M.J. John, and R.D. Anandjiwala, Mineralization of poly(lactic acid) (PLA), poly(3-hydroxybutyrate-co-valerate) (PHBV) and PLA/PHBV blend in compost and soil environments. *J. Renew. Mater.* **4**, 133–145 (2016).
3. O. Martin and L. Avérous, Poly(lactic acid): Plasticization and properties of biodegradable multiphase systems. *Polymer* **42**, 6209–6219 (2001).
4. J.M. Ferri, M.D. Samper, D. García-Sanoguera, M.J. Reig, O. Fenollar, and R. Balart, Plasticizing effect of biobased epoxidized fatty acid esters on mechanical and thermal properties of poly(lactic acid). *J. Mater. Sci.* **51**, 5356–5366 (2016).
5. N.M. Stark, Opportunities for cellulose nanomaterials in packaging films: A review and future trends. *J. Renew. Mater.* **4**, 313–326 (2016).
6. R. Sabo, A. Yermakov, C.T. Law, and R. Elhajjar, Nanocellulose-enabled electronics, energy harvesting devices, smart materials and sensors: A review. *J. Renew. Mater.* **4**, 297–312 (2016).
7. X. Xu, F. Liu, L. Jiang, J.Y. Zhu, D. Haagenson, and D.P. Wiesenborn, Cellulose nanocrystals vs. cellulose nanofibrils: A comparative study on their microstructures and effects as polymer reinforcing agents. *ACS Appl. Mater. Interfaces* **5**, 2999–3009 (2013).
8. J. Peng, T. Ellingham, R. Sabo, L.-S. Turng, and C.M. Clemons, Short cellulose nanofibrils as reinforcement in polyvinyl alcohol fiber. *Cellulose* **21**, 4287–4298 (2014).
9. U.P. Agarwal, R. Sabo, R.S. Reiner, C.M. Clemons, and A.W. Rudie, Spatially resolved characterization of cellulose nanocrystal-polypropylene composite by confocal raman microscopy. *Appl. Spectrosc.* **66**, 750–756 (2012).
10. D. Klemm, F. Kramer, S. Moritz, T. Lindström, M. Ankerfors, D. Gray, and A. Dorris, Nanocelluloses: A new family of nature-based materials. *Angew. Chem. Int. Ed.* **50**, 5438–5466 (2011).
11. A. Samir, M.A. Said, F. Alloin, and A. Dufresne, Review of recent research into cellulosic whiskers, their

properties and their application in nanocomposite field. *Biomacromolecules* **6**, 612–626 (2005).
12. K. Oksman, A.P. Mathew, D. Bondeson, and I. Kvien, Manufacturing process of cellulose whiskers/polylactic acid nanocomposites. *Compos. Sci. Technol.* **66**, 2776–2784 (2006).
13. Z. Zhang, G. Sèbe, D. Rentsch, T. Zimmermann, and P. Tingaut, Ultralightweight and flexible silylated nanocellulose sponges for the selective removal of oil from water. *Chem. Mater.* **26**, 2659–2668 (2014).
14. N.S. Çetin, P. Tingaut, N. Özmen, N. Henry, D. Harper, M. Dadmun, and G. Sèbe, Acetylation of cellulose nanowhiskers with vinyl acetate under moderate conditions. *Macromol. Biosci.* **9**, 997–1003 (2009).
15. E. Fortunati, I. Armentano, Q. Zhou, A. Iannoni, E. Saino, L. Visai, L.A. Berglund, and J.M. Kenny, Multifunctional bionanocomposite films of poly(lactic acid), cellulose nanocrystals and silver nanoparticles. *Carbohydr. Polym.* **87**, 1596–1605 (2012).
16. E. Fortunati, F. Luzi, D. Puglia, F. Dominici, C. Santulli, J.M. Kenny, and L. Torre, Investigation of thermomechanical, chemical and degradative properties of PLA-limonene films reinforced with cellulose nanocrystals extracted from phormium tenax leaves. *Europ. Polym. J.* **56**, 77–91 (2014).
17. V.T. Phuong and A. Lazzeri, "Green" biocomposites based on cellulose diacetate and regenerated cellulose microfibers: Effect of plasticizer content on morphology and mechanical properties. *Compos. Part A: Appl. Sci. Manuf.* **43**, 2256–2268 (2012).
18. L. Wei, U.P. Agarwal, K.C. Hirth, L.M. Matuana, R.C. Sabo, and N.M. Stark, Chemical modification of nanocellulose with canola oil fatty acid methyl ester. *Carbohydr. Polym.* **169**, 108–116 (2017).
19. R. Reiner and A. Rudie, Process scale-up of cellulose nanocrystal production to 25 kg per batch at the forest products laboratory, in *Production and Applications of Cellulose Nanomaterials*, M.T. Postek, R.J. Moon, A.W. Rudie, and M.A. Bilodeau (Eds.), p. 21, TAPPI Press, Peachtree Corners, GA (2013).
20. X. Lang, A.K. Dalai, N.N. Bakhshi, M.J. Reaney, and P.B. Hertz, Preparation and characterization of bio-diesels from various bio-oils. *Bioresource Technol.* **80**, 53–62 (2001).
21. L. Wei, N.M. Stark, R.C. Sabo, and L. Matuana, Modification of cellulose nanocrystals (CNCS) for use in poly(lactic acid) (PLA)-CNC composite packaging products, in *Proceedings of the Forest Products Society International Convention*, June 28–29, Portland, OR (2016).
22. L. Wei and A.G. McDonald, Peroxide induced crosslinking by reactive melt processing of two biopolyesters: Poly(3-hydroxybutyrate) and poly(l-lactic acid) improve their melting processability. *J. Appl. Polym. Sci.* **132**, 41724 (2014).
23. L. Wei, N.M. Stark, and A.G. McDonald, Interfacial improvements in biocomposites based on poly(3-hydroxybutyrate) and poly(3-hydroxybutyrate-co-3-hydroxyvalerate) bioplastics reinforced and grafted with α-cellulose fibers. *Green Chem.* **17**, 4800–4814 (2015).
24. L. Wei, A.G. McDonald, C. Freitag, and J.J. Morrell, Effects of wood fiber esterification on properties, weatherability and biodurability of wood plastic composites. *Polym. Degrad. Stab.* **98**, 1348 (2013).
25. V. Khoshkava and M.R. Kamal, Effect of cellulose nanocrystals (CNC) particle morphology on dispersion and rheological and mechanical properties of polypropylene/cnc nanocomposites. *ACS Appl. Mater. Interfaces* **6**, 8146–8157 (2014).
26. A.N. Frone, D.M. Panaitescu, I. Chiulan, C.A. Nicolae, Z. Vuluga, C. Vitelaru, and C.M. Damian, The effect of cellulose nanofibers on the crystallinity and nanostructure of poly(lactic acid) composites. *J. Mater. Sci.* **51**, 9771–9791 (2016).
27. B.W. Chieng, N.A. Ibrahim, W.M.Z. Wan Yunus, M.Z. Hussein, and V.S.G. Silverajah, Graphene nanoplatelets as novel reinforcement filler in poly(lactic acid)/epoxidized palm oil green nanocomposites: Mechanical properties. *Int. J. Mol. Sci.* **13**, 10920–10934 (2012).
28. M.R. Kamal and V. Khoshkava, Effect of cellulose nanocrystals (CNC) on rheological and mechanical properties and crystallization behavior of Pla/Cnc nanocomposites. *Carbohydr. Polym.* **123**, 105–114 (2015).
29. S. Sahoo, M. Misra, and A.K. Mohanty, Enhanced properties of lignin-based biodegradable polymer composites using injection moulding process. *Compos. Part A: Appl. Sci. Manufac.* **42**, 1710–1718 (2011).
30. M.P. Arrieta, E. Fortunati, F. Dominici, J. López, and J.M. Kenny, Bionanocomposite films based on plasticized PLA–PHB/cellulose nanocrystal blends. *Carbohydr. Polym.* **121**, 265–275 (2015).
31. L. Wei, A.G. McDonald, and N.M. Stark, Grafting of bacterial polyhydroxybutyrate (PHB) onto cellulose via in situ reactive extrusion with dicumyl peroxide. *Biomacromolecules* **16**, 1040–1049 (2015).
32. M. Zhai and G.B. McKenna, Elastic modulus and surface tension of a polyurethane rubber in nanometer thick films. *Polymer* **55**, 2725–2733 (2014).

Supplementary Document Available Online

http://www.scrivenerpublishing.com/journalsuppl/jrm/JRM-2017-0020/jrm_JRM-2017-0020_supp1.docx